Effects of Aquatic and Emergent Riparian Vegetation on SWOT Mission Capability in Detecting Surface Water Extent

Nicolas M. Desrochers, Mélanie Trudel, Sylvain Biancamaria, Gabriela Siles, Damien Desroches, Denis Carbonne, and Robert Leconte

***Abstract*—The future surface water and ocean topography (SWOT) satellite mission will provide images of surface water topography for inland water bodies and oceans. Over land, water surface elevation (WSE) will be retrieved at 10 cm accuracy for water bodies with areas $>$ 250 m $\times$ 250 m and rivers with widths $>$ 100 m, when averaging over 1 km^2. Studies have shown that the Ka-band used by SWOT's main payload can be affected by aquatic and emergent riparian vegetation, which in turn could influence SWOT capacity to correctly observe water extent. The current study investigates effects of aquatic and emergent riparian vegetation on SWOT water extent and WSE detection capabilities through the use of NASA/JPL's SWOT simulator (HR). Data from the AirSWOT airborne campaign over Mamawi Lake (163 km^2) in the Peace-Athabasca Delta (PAD, Alberta, Canada), are used to establish a land cover classification and backscattering values for simulation inputs. Simulation results have shown that aquatic vegetation has a negligible effect on the SWOT signal. Yet, simulations showed that water extent misclassification can occur for water with emergent riparian vegetation in the specific case of wetlands surrounding lakes (i.e., small differences in backscattering values between surrounding land and water with emergent riparian vegetation). Simulations featuring the smallest difference between emergent riparian vegetation and land (1.3 dB) showed a 32–35% lake extent reduction from true extent. As expected, this study reveals that estimating water extent from SWOT in very wet environments with emergent vegetation can be challenging.**

***Index Terms*—AirSWOT, aquatic vegetation, emergent vegetation, surface water ocean topography (SWOT).**

I. Introduction

FOR the last few decades, many technological advances have been made to help close regional water balances around the globe. Data are lacking in many areas of the world that would otherwise provide a greater global understanding of water balances. Notably, the installation and use of *in situ* gauge networks for measuring water discharge and levels have been on a decline in recent decades [1], [2] and water data are not always shared internationally. *In situ* gauging systems also have poor spatial resolution, which limits their applicability in monitoring large water bodies. Advances in remote sensing have helped bridge the gap in data acquisition for water resource purposes to a certain extent [3]. The use of traditional/existing nadir radar altimeters have enabled remotely sensed observations of water surface elevations (WSE) over poorly gauged regions and have helped complement *in situ* gauge networks [3]. Yet, the main limitations of such instruments are their coarse time sampling and spatial coverage. To overcome the latter, the surface water and ocean topography (SWOT) mission is being developed by the National and Space Administration (NASA) of the United States, the Centre National d'Etudes Spatiales (CNES, the French space agency), the Agence Spatiale Canadienne/Canadian Space Agency (ASC/CSA), and United Kingdom Space Agency (UKSA).

SWOT, the launch of which is scheduled for 2022, will offer a new perspective on acquiring critical data that are needed to complete the global water balance [4]. SWOT will have a Ka-band (35.75 GHz/8.6 mm) SAR interferometer sensor (KaRIn) with near-nadir incidence angle [5]. This will allow SWOT to observe WSE over water bodies with an extent that is equal to or greater than 250 m $\times$ 250 m and rivers that are greater than 100 m wide [6]. 10 cm accuracy on WSE is expected when averaging over 1 km^2 of water extent (vegetation excluded). SWOT is the first radar altimeter mission that will produce elevation imagery (over two 50-km wide swaths), rather than along-track water elevation measurements. Given SWOT's steep incidence angle of $\sim$0.6° to $\sim$3.9°, backscattered energy should be more intense over water bodies than over land [5]. With this difference in amplitude between water and land, a water mask can be computed. Yet, some surface roughness over water (ripples from wind) is still required to acquire a strong backscattering signal [8]. Biancamaria *et al.* [5] further describe SWOT's applications to inland hydrology.

To generate SWOT-like data, several simulators have been developed by NASA/Jet Propulsion Laboratory (JPL), each been

Manuscript received April 25, 2021; revised October 16, 2021; accepted October 31, 2021. Date of publication November 15, 2021; date of current version December 15, 2021. This work was supported in part by the U.S. Department of Commerce under Grant BS123456, and in part by the Canadian Space Agency under Grant 14SUSWOTSH. The works of Sylvain Biancamaria, Damien Desroches, and Denis Carbonne were supported by CNES. *(Corresponding author: Nicolas Desrochers.)*

Nicolas M. Desrochers, Mélanie Trudel, Gabriela Siles, Damien Desroches, and Robert Leconte are with the University of Sherbrooke, Sherbrooke, QC J1K 2R1, Canada (e-mail: nicolas.desrochers@usherbrooke.ca; melanie.trudel@usherbrooke.ca; gabriela.llanet.siles@usherbrooke.ca; damien.desroches@cnes.fr; robert.leconte@usherbrooke.ca).

Sylvain Biancamaria is with LEGOS, Université de Toulouse, 31400 Toulouse, France (e-mail: sylvain.biancamaria@legos.obs-mip.fr).

Denis Carbonne is with CNES, Centre Spatial de Toulouse, 31400 Toulouse, France (e-mail: denis.carbonne@cnes.fr).

Digital Object Identifier 10.1109/JSTARS.2021.3128133

This work is licensed under a Creative Commons Attribution 4.0 License. For more information, see https://creativecommons.org/licenses/by/4.0/

an updated version of its predecessor. Most publish studies used the 2016 version (build 1040) while earlier studies used an older version of the simulator. The differences between simulators are mainly bug-fixes and some hypothesis with backscattering (Sigma0) readjustment. More recently, a simplified large-scale simulator has also been developed to simulate the expected SWOT errors [7]. Use of SWOT-like data for Arctic lakes was first investigated by Lee *et al.* [8]. They analyzed the effects of SWOT vertical accuracy and time-interval sampling on Arctic lake storage changes, and error dependencies related to lake size. They simulated SWOT measurement errors as white noise. It was concluded that lake size and shape were the primary determinants of storage change accuracy. To further investigate SWOT errors over inland water bodies, NASA/JPL developed a realistic SWOT data simulator, which allowed representative SWOT measurement simulations. Solander *et al.* [9] described the first study using this simulator for lakes (taking into account only instrument and atmospheric errors) using an earlier version of the SWOT simulator. They evaluated the effect of SWOT measurement errors on monthly reservoir storage estimates over six reservoirs in California. Their results showed water storage errors less than 5% for lakes under 10 km^2 and less than 0.1% for lakes over 100 km^2. Surface water area and elevation errors ($<5\%$ and <15 cm, respectively) were minimal above 1 km^2, except for reservoirs that had substantial elliptical shapes that were parallel to orbits, that were surrounded by mountainous terrain, or had less than 30% swath coverage. Likewise, Bonnema and Hossain [10] used the simulator to analyze storage changes and showed that of 20 reservoirs tested in the Mekong River Basin, only three had errors that were greater than 8%. In those three instances, the surrounding topography was complex and features had long narrow shapes. Lastly, Grippa *et al.* [11] obtained simulated WSE over Sahelian ponds with a 4 cm accuracy for round-shaped lakes with areas ranging from 100 to 250 ha. For water bodies with more elongated shapes, they found higher errors with WSE accuracy between 6.3 to 15.1 cm. All of these studies confirmed that lake size and shape would have an effect on SWOT WSE accuracy and estimated water storage changes.

Different sources of error are taking into consideration for the SWOT mission. As describe by Esteban-Rodriguez [12], a 10 cm height error is compounded from sources likes atmospheric disturbance, radial, and motion errors as well as systematic error after cross-over corrections. However, some sources of error are not compiled in the 10 cm, mostly environmental sources of error such as rain, which was shown to have significant impact on Ka-band signal [13]. As such, quality flags are put in place to inform the user of potential issues with the data. Currently, quality flags will be available for rain, ice, and topographic layover. However, there are presently no flags for vegetation.

In addition to the SWOT simulator, NASA/JPL launched the airborne mission AirSWOT, which flew in the context of the Arctic Boreal Vulnerability Experiment (ABoVE) in northern Canada and Alaska [14]. AirSWOT carries a SWOT-like Ka-band instrument (KaSPAR), which operates with two swaths (0 to 6° and 4 to 25° incidence angles), and a colour-infrared camera with 1-m spatial resolution. So far, AirSWOT has been used to validate the near nadir-looking Ka-band bistatic interferometry SAR instrument concept for measuring WSE [15]–[17], and in estimating river discharge [18] and water masks [19]. Validation of AirSWOT measurements was first accomplished by Altenau *et al.* [15] by comparing the WSE and slope *to in-situ* data on the Tanana River (Yukon, Alaska). A root-mean-square error (RMSE) of 9 cm for WSE over 1 km^2 and of 1 cm km^{-1} for slope along a 10-km reach were achieved, making AirSWOT a possible SWOT validation measurement. AirSWOT measurement validation was also tested on lakes and rivers by Pitcher *et al.* [20] in the Yukon Flats (Alaska). An RMSE of 8 cm over 1 km^2 was attained on rivers, but a 21-cm RMSE was exhibited for lakes, which falls short of SWOT's science requirements for 10 cm over 1 km^2 [6]. The authors explain that the poor results on lakes could be improved with advances to the AirSWOT InSAR processor and calibration data.

One of the notable advantages of the Ka-band, used in KaRIn, when compared to lower frequencies (especially Ku-band used by most nadir altimeters), is that it allows finer spatial resolution for SAR processing [5]. Yet, its frequency has weaker vegetation penetration capability when compared to sensors operating at lower frequencies, such as the C- or L-bands [21]. This is especially true when observing areas of flooded vegetation. In a review on SAR-based detection of flooded vegetation, Tsyganskaya *et al.* [22] summarized 128 articles that mainly focused on the L-band, C-band, and X-band, with incidence angles varying between 10° and 65°. They noted that signal penetration depended mostly upon vegetation density. Higher frequencies (e.g., X-band) proved to have the greatest difficulty in mapping flooded extents due to volume scattering from tree leaves, while showing some improvement during leafless seasons. In terms of incidence angle, steeper angles (nearer to nadir) were shown to have fewer interactions with the vegetation canopy and, therefore, could better distinguish between flooded and nonflooded areas of vegetation. Current SAR missions (e.g., TERRASAR-X, RADARSAT) are also used to do SAR interferometry (InSAR). Many have shown good result for water level retrieval in wetland environments [23]. Water level measurements are also possible in flooded or emergent vegetations areas due to the double-bounce backscattering mechanism, which produces the high coherence values needed for good quality InSAR measurements [23]. However, these missions operate at a much lower radar frequency and higher incidence angles ($\sim$20° to 60°) than SWOT (0.6° to 3.9°). Even if SWOT is an InSAR mission, it should not be expected to interact in the same way with flooded vegetation as other SAR missions, because it operates in Ka-band with very low (i.e., near nadir) incidence angles. To our knowledge, the performance of the Ka-band at near-nadir incidence angles for flooded vegetation has yet to be assessed. Therefore, it is uncertain how SWOT's detection capability will react to areas of flooded or emergent vegetation. Fayne *et al.* [24] have recently investigated the interactions of the Ka-band signal with various natural land covers using the AirSWOT mission. Preliminary results from Fayne *et al.* [24] have shown that at steep incidence angles, the intensity of the return signal was greatest over open water, but decreased over emergent riparian vegetation and was lower still over dry land.

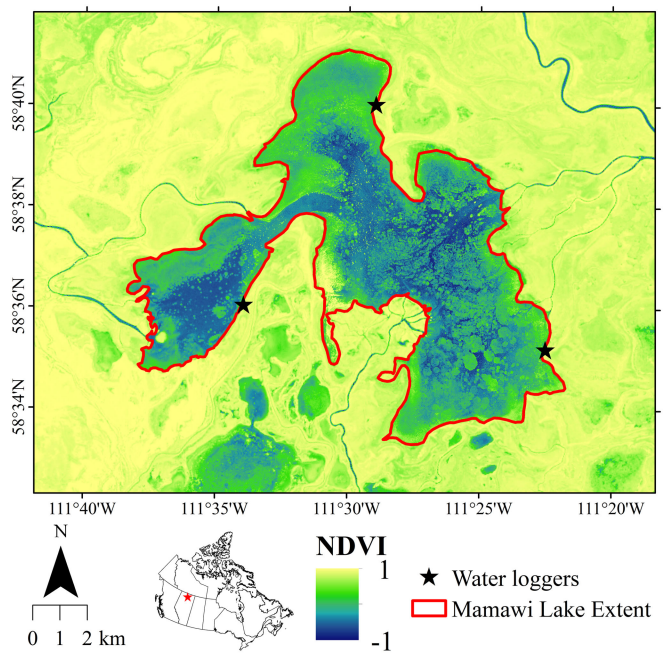

Fig. 1. Map and location of Mamawi Lake. The red line shows RADARSAT 2 open water extent. AirSWOT NDVI values that are closer to 1 show a higher intensity of vegetation, while −1 shows a lack of vegetation.

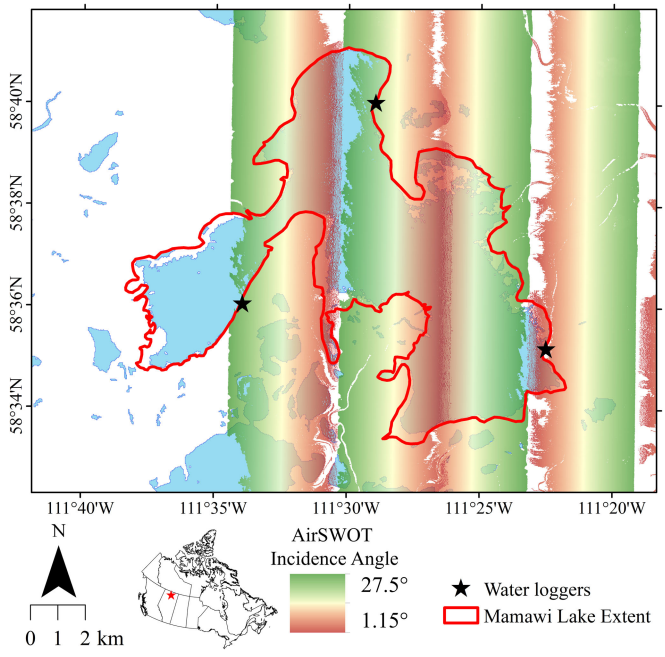

Fig. 2. Map of AirSWOT passage with incidence angle value (green to red colours).

However, they noted that signal strength over dry land increased with increasing soil moisture content.

Still, no study has focused upon the sensitivity of the SWOT signal over aquatic or emergent riparian vegetation, especially in wet environments where soil moisture content is high. SWOT signal attenuation over aquatic and emergent riparian vegetation might affect the SWOT data-processing chain, resulting in misclassification of water as land, thereby underestimating total water extent. This study focuses upon the effect of aquatic and emergent riparian vegetation on the SWOT classification process using the NASA/JPL SWOT-HR simulator and its effects on the surface water extent and WSE. To do so, various land cover composition scenarios were run through the simulator using AirSWOT-derived backscattering values. This study hints at some of SWOT's blind spots concerning inland lake hydrology.

II. Description of the Study Area and Data

A. Mamawi Lake

Mamawi Lake is located in the Peace-Athabasca Delta (PAD) of Northern Alberta, Canada (shown in Fig. 1). The PAD is considered to be one of the world's largest inland deltas and is composed of a complex hydrographic network with many interconnected and isolated lakes with flow reversals frequently occurring due to its flat topography [25]. The land surrounding Mamawi Lake is very flat and typically very wet. This sector has previously been used for SWOT research [26], [27]. The extent of Mamawi Lake varies greatly with fluctuations in WSE, as it extends well into the riparian vegetation at high WSE levels Further details regarding WSE fluctuation in the PAD are found in Peters *et al.* [25]. The lake extends up to 10 km at its greatest width and less than 1 km at its narrowest. The lake is also very shallow; its deepest area is only 2 m. Aquatic vegetation can cover a substantial area of the lake depending upon the time of the year. Fig. 1 shows the Normalized Difference Vegetation Index (NDVI) of Mamawi Lake with its surface water extent on 13 August 2017, when AirSWOT data were acquired (see Section II-B below). On this date, aquatic vegetation covered nearly 50% of the lake's surface.

B. Data

This study uses an AirSWOT dataset featuring four passes that were acquired on 13 August 2017 (Fig. 2), which are freely available at[1] The dataset consists of colour-infrared images (a sensor that SWOT will not carry), SAR backscattering values (magnitude), incidence angle and elevation at 1 m spatial resolution. The colour-infrared images were used in the land classification process (further description in Section III-A). Given that AirSWOT coverage did not extend to the western part of the lake, a Landsat 8 image (30 m spatial resolution; 10 August 2017) was used to complete the colour-infrared map. A RADARSAT-2 image from 24 August 2017 was also used in the land cover classification process to retrieve areas of open water and emergent riparian vegetation (Section III-A). Magnitudes and incidence angles from the AirSWOT data were used to retrieve backscattering values that served as input to the simulator (described in Section III-B). Fig. 2 shows AirSWOT coverage and incidence angles. It should be noted that the AirSWOT backscattering values did not show signs of double-bounce backscattering in emergent vegetation in contrast to other

[1][Online] Available: https://daac.ornl.gov/ABOVE/guides/ABoVE_AirSWOT_Radar_Data.html

InSAR missions due to AirSWOT's low incidence angles angles (as previously discussed in Section I). SWOT is expected to show similar backscattering values to AirSWOT for the same incidence angles independently of the altitude difference.

Surface water extent for the AirSWOT acquisition data was 163.79 km^2 as calculated with RADARSAT-2 (see Section III-A). *In situ* WSE and bathymetry were obtained during summer 2017 fieldwork. Three water loggers were deployed at different locations around the lake (shown in Fig. 1) and their averaged WSE measurement is equal to 209.35 m ($\pm$ 0.03 m, with reference to CGVD2013) on AirSWOT data acquisition day. Last, a Digital Elevation Model (DEM) with 2-m resolution was obtained from LiDAR missions over the PAD [26]. Bathymetry, *in situ* WSE, and DEM were used as inputs to the SWOT simulator and are described in Section III-B.

III. Methodology

The methodology that was used to simulate SWOT observations is presented in Fig. 3 and consist of four major steps described in the following subsections (each step corresponds to a different colour in Fig. 3).

A. Land Cover Classification

The goal of the land cover classification was to delineate areas of open water, aquatic vegetation, Fig. 4 emergent riparian vegetation, and dry land to define the input scene to the SWOT simulator (blue boxes in Fig. 3). First, thresholding the RADARSAT-2 backscatter image below -0.52 dB (based upon visual inspection) allowed us to retrieve the limits of open water. Since RADARSAT-2 is in the C-band (5.405 GHz), the satellite's signal is not affected by aquatic vegetation. To delineate aquatic vegetation, a normalized difference vegetation index (NDVI) was calculated using the AirSWOT colour-infrared camera within the open water mask from RADARSAT-2. The NDVI for the western portion of the lake, which is missing from the AirSWOT data, was completed using a Landsat 8 image. It should be noted that there is a significant difference in spatial resolution between Landsat 8 and the AirSWOT Colour image (30 and 1 m, respectively).

Emergent riparian vegetation extent was delineated using the RADARSAT-2 double bounce backscattering mechanism, which occurs in flooded or emergent vegetation when the signal bounces off the water and vegetation. This interaction generates high backscattering values that can be mapped visually or with the used of algorithms [22]. For this study, visual interpretation was used to delineate the double-bounce backscattering. The remaining of the lake's study frame is classified as "land." Fig. 5 shows the final land cover classification. It should be noted that river reaches in and out of Mamawi Lake are not considered and are classified as emergent riparian vegetation for the sake of simplicity.

B. Input to Simulator

Prior to running the simulator, the data need to be assembled in a manner that can be read by the SWOT simulator (green boxes in Fig. 3). First, the DEM and bathymetry are combined with the observed WSE at the time of the AirSWOT pass over Mamawi Lake. This input data are used as a three-dimensional reference model of the lake water elevation and surroundings. This was accomplished by simply assigning a constant surface

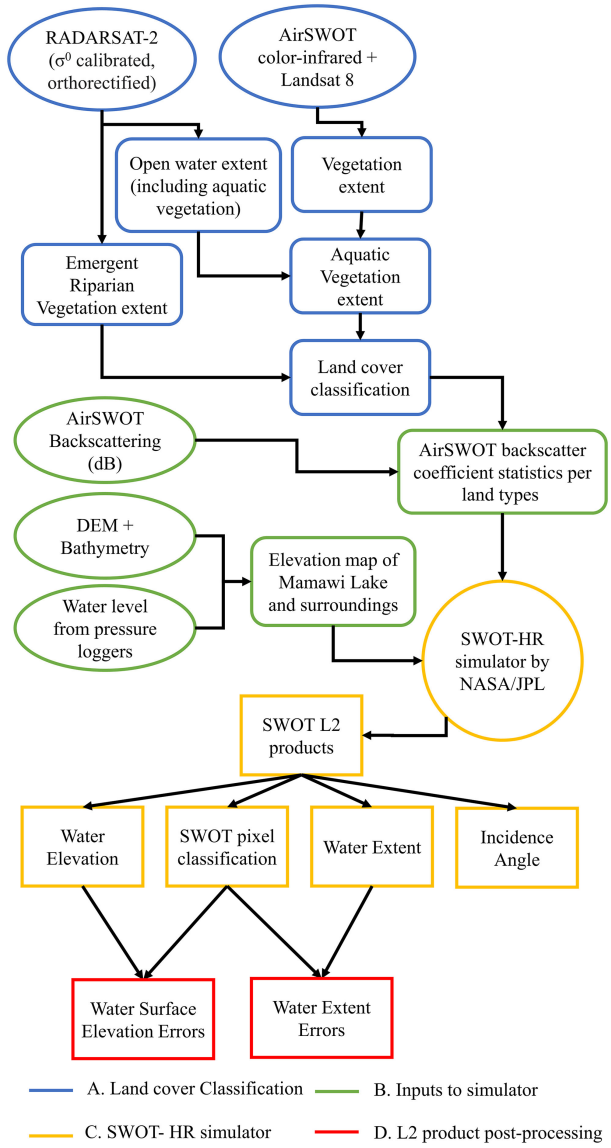

Fig. 3. Systematic workflow for data processing as input to the SWOT simulator.

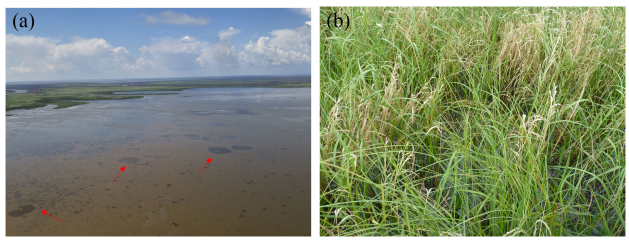

Fig. 4. Photographs of aquatic vegetation that are indicated with red arrows (A), and emergent riparian vegetation (B) in Mamawi Lake and its surroundings.

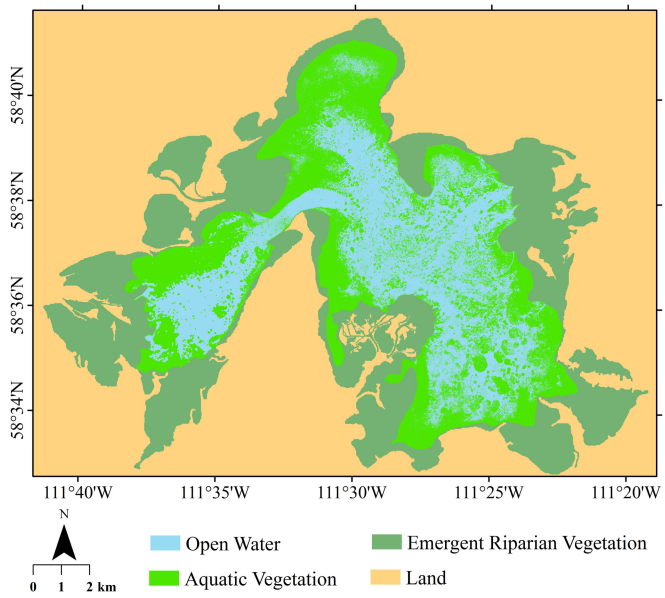

Fig. 5. Land cover classification from AirSWOT and RADARSAT-2 data.

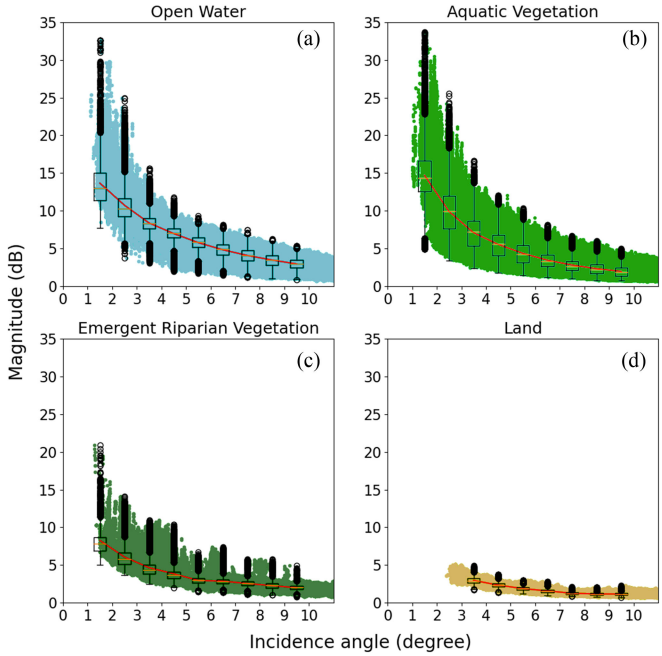

Fig. 6. AirSWOT backscattering distribution versus incidence angle for all land cover classifications. Red lines show the mean backscattering value of each pixel for a given range of incidence angles (1° bins have been considered).

water elevation value from an averaging of the three water loggers measurements (see Fig. 1 for their locations) to all pixels in the DEM/bathymetry data that fell below that value within the lake boundaries.

Second, the SWOT simulator requires land cover with associated backscattering values. For each land cover type in the land cover classification (described in Section III-A), the distribution of intensity values (dB) is retrieved from the AirSWOT backscattering intensity data. The distribution of backscattering values for each land cover vs incidence angle is shown in Fig. 6;

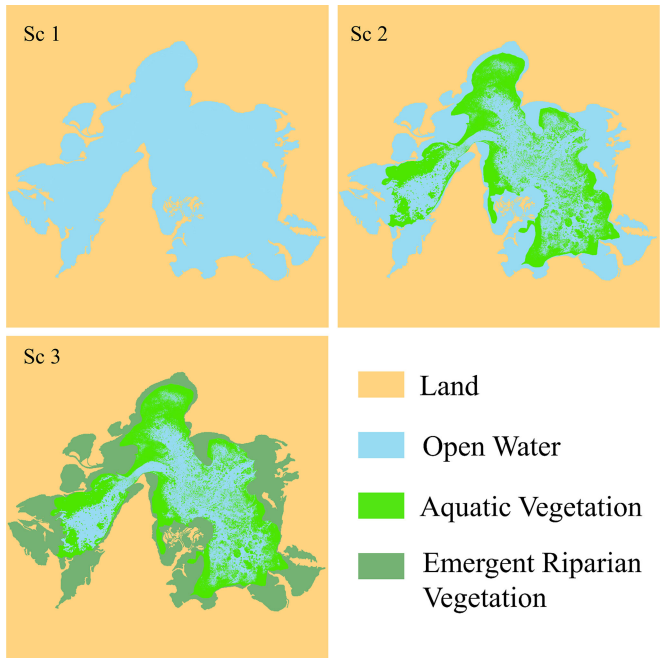

Fig. 7. Land cover composition of each scenario.

box-and-whisker plots are superimposed upon these values at the mid-points between each incident angle interval. Open water [Fig. 6(a)] has the highest values at steep incidence angles, followed closely by aquatic vegetation [Fig. 6(b)], then emergent riparian vegetation [Fig. 6(c)] and land [Fig. 6(d)]. The range of the distributions varies greatly depending upon the land cover, with an interquartile range (IQR, 25th to 75th percentile) of $\sim$4 dB for open water and aquatic vegetation and $\sim$2 dB and $<$ 1 dB for emergent riparian vegetation and land, respectively. Values of the distributions by land cover emerge shortly after 1°, except for dry land, which begins around 2.5°. When comparing the median (50th %) within SWOT incidence angles ($\sim$0.6° to $\sim$3.9°) of open water and land distributions, there is a difference of $\sim$10 dB. This is comparable with the 10 to 20 dB water/land contrast that was observed by Fjortoft *et al.* [21], which is the default water/land contrast of the SWOT-HR simulator.

Since the goal of the study is the analyze the effect of both aquatic and emergent riparian vegetation on SWOT's products, three scenarios were created featuring different land cover combinations. The first scenario (Sc1) only has two classes: open water and land. In this case, the aquatic and emergent riparian vegetation are considered part of the open water. This scenario acts as a reference, providing expected SWOT errors on the study domain with no vegetation and is further on referred to as the "true extent." The second scenario (Sc2) adds the extent aquatic vegetation to the first scenario, while maintaining the emergent riparian vegetation extent as open water. In this scenario, aquatic vegetation can be evaluated without the potential influence of the emergent riparian vegetation. The third scenario (Sc3) considers all land cover types. This last scenario serves as the most realistic scene seen by SWOT. Fig. 7 shows the spatial distribution of the land cover types for each scenario.

Furthermore, subscenarios are also used to simulate the effect of varying backscattering values within a particular scenario. Table I compiles 10 subscenarios that were used in this study and the attributed backscattering value for each land cover. The chosen intensity values used for each subscenario are constrained within 0° to 4° of AirSWOT's incidence angle, except for the "land" classification, where measurements only start at ∼2.5°. To vary intensity values between the subscenarios, a combination of the 25th and 50th percentiles from each land cover distribution were used as input to the SWOT simulator. Fayne *et al*. [24] showed that backscattering values between land and emergent riparian vegetation can sometimes merge; the 75th percentile of backscattering values was not used to maintain a conservative approach to the simulations, while keeping them realistic. The values that were used for the simulation are static across land cover type and do not vary with incidence angle. This choice was made to simplify the simulations and to focus upon the SWOT classification process.

Scenario 1 has two subscenarios (sc1.1 and sc1.2). Sc1.1 corresponds to the default simulator intensity values (10 dB for open water and −5 dB for land) and is comparable with previous studies, which used the SWOT simulator. For Sc1.2, AirSWOT intensity values are used instead of the default simulator values. The 50th percentile intensity value of both open water and land is used as input to the simulator (9.11 and 3.03 dB, respectively). This sub-scenario serves as a base simulation to compare all other simulations.

Scenario 2 has three subscenarios (sc2.1, sc2.2, sc2.3) and focuses on aquatic vegetation. Like Sc1.1, Sc2.1 uses default open water and land simulator intensity value to test the incorporation of a third land cover. Since most studies using the simulator had only an open water and land classification, aquatic vegetation was arbitrary set to 5 dB value to test the addition of a third land cover classification. Sc2.2 uses the 50th percentile from AirSWOT aquatic vegetation intensity value, while Sc2.3 uses the 25th percentile for aquatic vegetation intensity only. For scenario 2, land intensity value is left at the simulator default value for all subscenarios to minimize the contrast between land and aquatic vegetation in order to focus on the interaction of aquatic vegetation and open water.

Scenario 3 had five subscenarios (Sc3.1, Sc3.2, Sc3.3, Sc3.4, and Sc3.5) and simulates the realistic land cover extents. Sc3.1 and Sc3.2 use the 50th and 25th percentiles of AirSWOT intensity values for emergent riparian vegetation, respectively. Land intensity value is kept at the default simulator value to focus on differences between open water, aquatic vegetation, and emergent riparian vegetation. Sc3.3 tests the effect of emergent riparian vegetation without any potential impact from the aquatic vegetation. To do so, aquatic vegetation intensity value is set with open water values. Lastly, Sc3.4 and Sc3.5 are using AirSWOT intensity values for the "land" class. Sc3.4 and Sc3.5 simulate with 25th and 50th percentiles of AirSWOT intensity value for this class, respectively.

It should be noted that the intensity value attributed to the "land" class is set to the default simulator value (non-AirSWOT) of −5 dB for most sub-scenarios except Sc1.1, Sc3.4, and Sc3.5 (Table I). The goal of the scenarios with default "land" class values is to focus on the contrast of vegetation and open water.

TABLE I
DISTRIBUTION OF BACKSCATTERING VALUES FOR EACH SCENARIO BASED UPON AIRSWOT BACKSCATTERING

	Open Water (dB)	Aquatic Vegetation (dB)	Emergent Riparian Vegetation (dB)	Land (dB)
Sc 1.1	10	10	10	-5
Sc 1.2	9.11	9.11	9.11	3.03
Sc 2.1	10	5	10	-5
Sc 2.2	9.11	8.52	9.11	-5
Sc 2.3	9.11	6.32	9.11	-5
Sc 3.1	9.11	8.52	5.21	-5
Sc 3.2	9.11	8.52	4.33	-5
Sc 3.3	9.11	9.11	4.33	-5
Sc 3.4	9.11	8.52	4.33	3.03
Sc 3.5	9.11	8.52	5.21	3.03

Colours refer to land cover combination. Blue: without vegetation; green: aquatic vegetation only; orange: aquatic and emergent riparian vegetation. All values are in dB.

TABLE II
RMSE BETWEEN SIMULATED SWOT WSE AND TRUE WSE, AND THE DIFFERENCE BETWEEN SWOT LAKE EXTENT AND THE TRUE LAKE EXTENT EXPRESSED AS A PERCENTAGE OF TRUE LAKE EXTENT

	RMSE (m)		AREA %	
Pass	**25**	**303**	**25**	**303**
Sc 1.1	0.06	0.08	1.1	-8.5
Sc 1.2	0.07	0.08	1.0	-9.4
Sc 2.1	0.08	0.09	0.9	-8.6
Sc 2.2	0.09	0.12	1.1	-8.4
Sc 2.3	0.09	0.25	1.1	-8.4
Sc 3.1	0.18	0.30	-1.4	0.3
Sc 3.2	0.14	0.27	-18.3	-6.2
Sc 3.3	0.14	0.27	-18.2	-6.1
Sc 3.4	0.10	0.13	-35.0	-32.4
Sc 3.5	0.14	0.26	-13.2	-7.6

C. SWOT-HR Simulations

As stated in Section I, NASA/JPL developed the SWOT-HR simulator, which produces synthetic SWOT Single Look Complex (SLC) data over a given area. This study used the simulator version from September 2019. Further details on the simulator can be found in, Domeneghetti *et al.* [28] and Durand *et al.* [29]. Input to the simulator consists of digital elevation model (DEM) with WSEs and the land cover classification (Fig. 3: blue and green boxes) with their associated backscattering values. The SLC simulator and its associated processing chain outputs three levels of data processing (L0, L1, and L2). The simulator

directly produces two SLC from each KaRiN antenna, and the L2 interferometric processing chain is then used to compute the geolocated heights (from the interferometric phase) and the pixel classification (from the SLC intensities). This study solely focuses upon L2-level Pixel Cloud products (Fig. 3: orange boxes). This product consists of a pixel cloud with many attributes that are associated with each pixel, such as WSE, water extent, incidence angle, classification (hereafter, referred to as the SWOT classification), and longitude/latitude coordinates. In the SWOT classification, pixels can be classified as: open water (OP); water near land (WNL); land near water (LNW); land (L); dark water (DW); dark water near land (DNL); and land near dark water (LND). Dark water occurs when there is an absence (or very little) signal return due to low surface roughness that is caused by low wind presence. The SWOT simulator generates dark water from random wind fields that are mapped through a geophysical model function, which returns backscattering values as a function of wind speed and incidence. Also, the simulator generates a layover effect, which is a phenomenon that arises when multiple radar signal (due to targets at different elevations) return to the sensor simultaneously, thereby distorting the images [21]. This effect usually occurs when the terrain slope is steeper than the incidence angle of the radar satellite. Since the PAD is very flat, layover was minimal and, therefore, it was not considered in the analyses. Further details regarding layover effects on SWOT are discussed by Durand *et al.* [29]. Different typical random errors in SWOT measurements (random noise error, layover, dark water, among others) are also considered in this SWOT simulator. Systematic errors are low frequency errors due to rolling residual errors. These and tropospheric errors are not considered in this study.

D. Pixel Cloud Product Postprocessing

Two attributes of the L2 pixel cloud product were used to evaluate effects of aquatic and emergent riparian vegetation on SWOT classification: area (extent of a given pixel) and elevation (height measurement of a given pixel), as shown by the red boxes in Fig. 3.

First, all subscenarios were filtered to retain only pixels that are within the true extent of both WSE and water extent. To compute WSE error, the simulated SWOT elevation data are first filtered, retaining only pixels that were classified as OP and WNL. Note that DW and DNL are not used for WSE error calculations because of increased errors that can be attributed to the simulated DW process. The difference between SWOT WSE and the input scene WSE (i.e., 209.35 m) is then computed for each pixel. Finally, WSE error corresponds to the RMSE of this difference over all selected pixels.

The simulated water extent error for each sub-scenario is calculated as a percentage of the true extent (163.79 km^2). In this case, pixels that were classified as OP, WNL, DW, or DNL are used for the water extent calculations. The addition of DW and DNL is required to complete the water extent and avoid random holes. The sum of each pixel group in each subscenario is then calculated to obtain the total water extent of each subscenario, which can then be expressed as a percentage of the true extent.

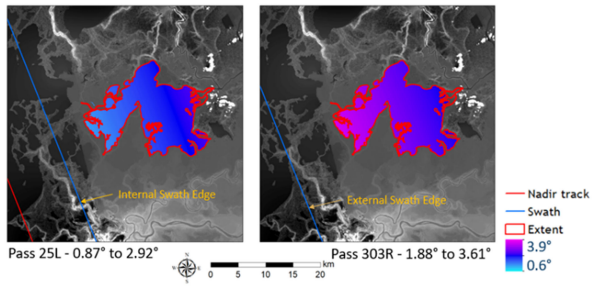

Fig. 8. SWOT incidence angle coverage over the lake for Pass 25 (left panel) and Pass 303 (right panel).

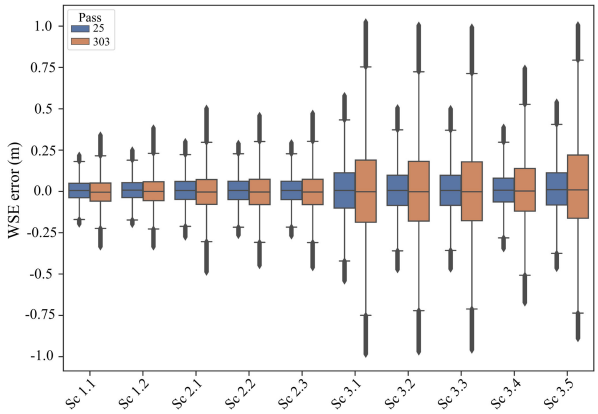

Fig. 9. Box-and-whisker plots of OP and WNL WSEs of L2 distributions of Pass 25 and Pass 303 scenarios.

IV. Simulation Results

A. Orbital Pass

Of the five orbital passes that were simulated, only two had full coverage of Mamawi Lake (Pass 25 and Pass 303). As depicted in Fig. 8, the two passes cover a different range of incidence angles. Pass 25 has the steeper angle (nearer to nadir). These two passes correspond to a descending track. The lake is located within Pass 25's left and Pass 303's right swath.

B. WSE

As mentioned in Section III-C, the L2 product consists of a pixel cloud with multiple attributes (e.g., WSE, water extent, classification, coordinates). Similar trends are demonstrated for Sc1s and Sc2s in both passes, whereas errors for Sc3s have a larger interquartile range (Fig. 9). Pass 303 has an interquartile range (25th to 75th percentile) that is noticeably larger than that of Pass 25 for all scenarios. Table II provides RMSE between pixel cloud water elevation that is filtered with the method presented in Section III-D and the true water elevation. For Pass 25, there is a 0.03 m RMSE increase between Sc1s and Sc2s (0.06 m to 0.09 m), while Pass 303 shows a 0.04 m increase between the same subscenarios (0.08 m to 0.12 m), except for Sc2.3 (0.25 m). Both passes have higher RMSE for Sc3s, averaging 0.14 m for Pass 25 and 0.25 m for Pass 303. Sc3.4 does exhibit a smaller RMSE than the rest of Sc3s for both Pass 25 and Pass 303 (0.10 and 0.13 m, respectively).

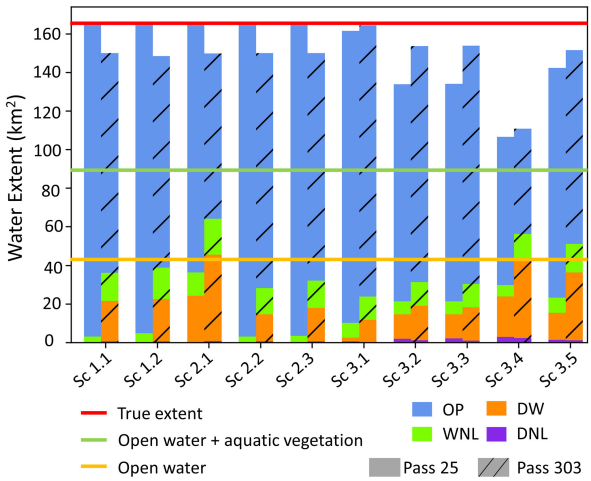

Fig. 10. Water extent comparison of Pass 25 (plain bars) and Pass 303 (striped bars). The red line indicates true water extent. The green line shows water extent without emergent riparian vegetation. The orange line only shows the open water extent.

C. Water Extent

The total water extent for each subscenario was calculated using the sum of water extent for all L2 filtered pixels, as explained in Section III-D. Fig. 10 shows the sum of all water extents for each simulation, for Pass 25 and Pass 303. Most of the total extent originates from OP pixels, followed by DW, WNL, and DNL. It is also worth noting that for Pass 303, water extent is underestimated, due to more DW than Pass 25, as shown by the orange colouring in Fig. 10. Further, SWOT lake water extent for Pass 25 has about a +1% difference with the true lake extent (red line in Fig. 10) for Sc1s and Sc2s (Table II). For Pass 303, SWOT lake extent is, on average, 8.7% smaller than the true lake extent for the same scenarios. Regarding the Sc3s, SWOT lake extents for Pass 25 are smaller for Sc3.2, Sc3.3, Sc3.4, and Sc3.5 (−18.3%, −18.2%, −35%, and −13.2%, respectively), which is not the case for Sc3.1, i.e., only a −1.4% difference from true lake extent. Pass 303 shows a trend slightly differing from Pass 25, where lake extents of Sc3.2 (−6.2%) and Sc3.3 (−6.1%) are closer to true extent than is Sc3.5 (−7.6%). Yet, the best result for Pass 303 is obtained with Sc3.1 (0.3% difference in water extent) and the smallest extent result is obtained with Sc3.4 (−32.4%). Furthermore, Sc3s results for Pass 303 (except Sc3.4) are closer to true extent (red line in Fig. 10) than are Sc1s and Sc2s. This is not the case for Pass 25. Sc 3.4 lake extent percentage is the lowest for both passes and is closer to open water plus aquatic vegetation extent (the green line in Fig. 10).

V. Discussion

A. Aquatic Vegetation

The aquatic vegetation was evaluated by comparing the Sc1s (with only "open water" and "land" classes in the land cover classification) and Sc2s (with "open water," "aquatic vegetation," and "land" classes in the land cover classification). The WSE RMSE of Sc1s (i.e., no aquatic or emergent riparian vegetation) are within the range of similar studies, such as Bonnema *et al.* [10], who estimated RMSEs ranging from 0.013 to 0.530 m. In this particular case, higher values were due to layover errors, which is not the case in our study, whereas Mamawi Lake is surrounded by very flat topography.

The results show a slight increase in RMSE between Sc1s and Sc2s for both passes. Pass 303 exhibits a slightly higher RMSE than Pass 25 for Sc1s and Sc2s (± 0.02 m), except for Sc2.3, which shows a 0.14 m difference in favour of Pass 303. Given that Pass 303 covers higher incidence angles (1.88° to 3.61°) than does Pass 25 (0.86° to 2.92°), RMSE differences between the two passes would indicate an increasing potential error with increasing incidence angle. Indeed, SWOT's mission performance and error budget documents [30] indicate that the error budget changes within a swath and is dependent of the incidence angle. Observations that are closer to the external border of the swath are bound to have more errors. The increase in RSME between Sc1s and Sc2s would indicate a slight effect of aquatic vegetation on WSE retrieval by SWOT. The difference is quite small, and it is questionable whether SWOT error would be increased beyond the 10 cm over 1 km^2 averaging, as specified in the SWOT science requirements. Aquatic vegetation is generally encountered within the open water limits and very rarely next to land. In the case of Mamawi Lake, a zone of emergent riparian vegetation separated aquatic vegetation from the land, thereby limiting the contrast between aquatic vegetation and land. It could be guessed that other lakes with the presence of aquatic vegetation next to land might exert a stronger effect on the SWOT signal. However, given the difference in backscattering values between aquatic vegetation and the land (∼5 dB from AirSWOT data), this situation seems unlikely to have an effect.

In terms of water extent, both passes have very similar percentage trends between Sc1s and Sc2s, with differences between SWOT and true lake water extents averaging 1% for Pass 25 and −8.5% for Pass 303. Sc1.2 hosted a different land backscattering value (3.03 dB), but does not show marked differences with Sc1.1 (no difference for Pass 25; 0.9% difference for Pass 303). The highest error for Pass 303 compared to Pass 25 is due to a misclassification of certain areas along the shore. As illustrated in Fig. 11 (Sc1.2 and Sc2.2), several areas on the lakeshore (most notably northwest and south) have several patches of SWOT that were classified as land pixels within the true extent. Since these areas are misclassified only in Pass 303, they are unlikely to be attributed to aquatic vegetation; rather, a more like explanation is the difference in incidence angle and associated error budget within the swath.

There are differences in the SWOT pixel classification distributions between the two passes. Indeed, Pass 303 has a larger portion of its water extent originating from dark water (Fig. 10, shown in orange) than Pass 25. It is expected that more dark water would be seen in the far range of SWOT (Pass 303), given that dark water is based upon randomly generated combinations of wind speed and incidence angle (as described in Section III-C). Furthermore, the incidence angle plays a role in the total simulated water extent since pixels with steeper incidence angles have increased extent values relative to pixels with higher incidence angles. This would explain the reduced water extent of Pass 303, which has a higher incidence angle (1.88° to 3.61°) than Pass 25

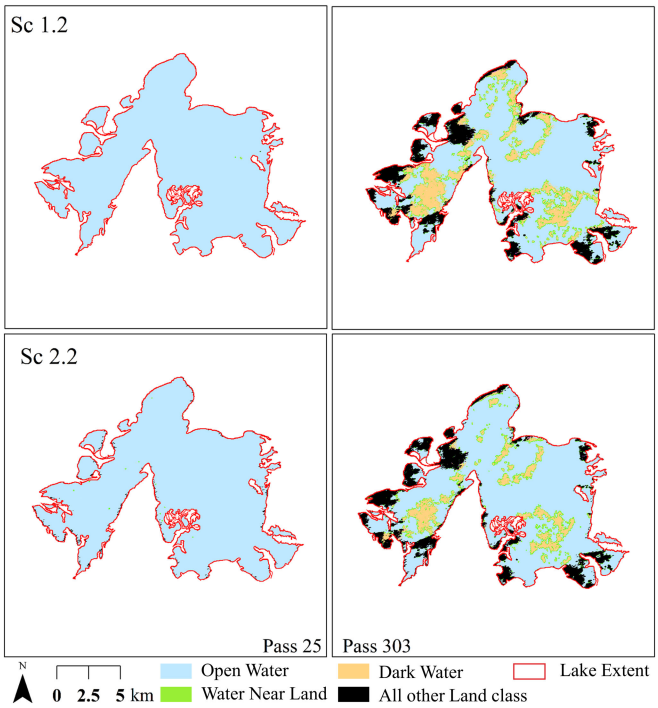

Fig. 11. Map of SWOT level 2 water classification within the true lake polygon from Sc1.2 (top panels) and Sc2.2 (bottom panels) for Pass 25 (left panels) and Pass 303 (right panels).

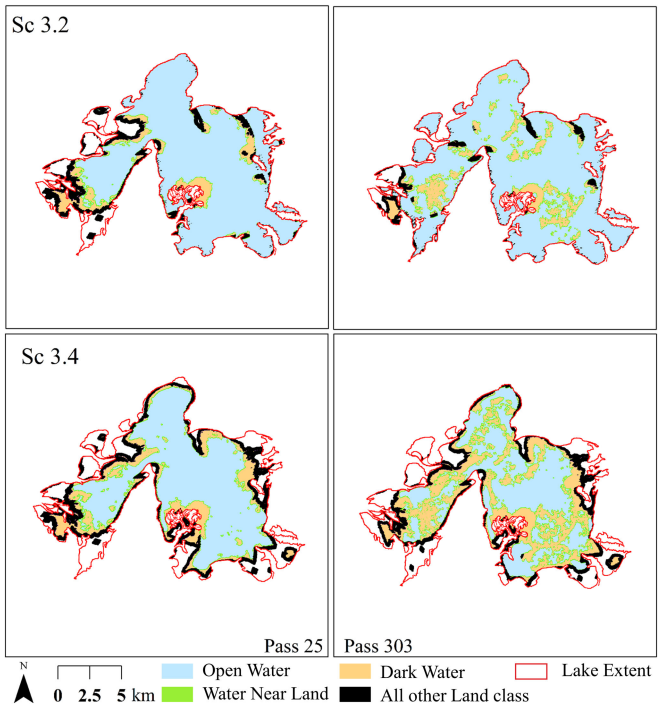

Fig. 12. Map of SWOT Level 1 water classification within the true lake polygon from Sc3.2 (top panels) and Sc 3.4 (bottom panels), for Pass 25 (left panels) and Pass 303 (right panels).

(0.87° to 2.92°). Therefore, misclassification at high angles of incidence would have more impact than at lower angles of incidence. Both Sc3.2 and Sc3.3 have emergent riparian vegetation, but they have different backscatter values for aquatic vegetation. Yet, they have identical water extent within each pass. The main difference that distinguishes the two is that Sc3.3 has the same backscatter value for aquatic vegetation and open water. Such differences between passes have also been observed in other studies [11]. These results suggest that aquatic vegetation would have little effect on the water detection capabilities of SWOT.

B. Emergent Riparian Vegetation

As presented in Section IV-C, emergent riparian vegetation was evaluated with the Sc3s. Both passes show an increase in WSE RMSE in Sc3s over those of Sc1s and Sc2s. As was pointed out in Section V-A, the difference between the two passes could be attributed to differences in incidence angle distributions between them. The increase in WSE RMSE for Sc3s in both passes could indicate a potential lake WSE error increase when there is wide coverage of emergent riparian vegetation. However, error values that are presented are relatively small and would unlikely influence WSE retrieval from SWOT science requirements of 10 cm over a 1 km^2 averaging. Still, it should be noted that Sc3.4 had the lowest RMSE for both passes. This scenario has a very small difference in backscattering values between land cover that is as classified emergent riparian vegetation (4.33 dB) and land (3.03 dB). It also exhibits the lowest water extent percentage (−35% for Pass 25 and −32.4% for Pass 303).

As stated in Section IV-C, both passes exhibit similar trends in Sc3s (Pass 25 at −1.4%; Pass 303 at 0.3%). Sc3.1 displays a water extent percentage close to true extent, which then decreases substantially in Sc3.2 (Pass 25 at −18.3%; Pass 303 at −6.2%) and Sc3.3 (Pass 25 at −18.2%; Pass 303 at −6.1%) to attain its lowest extent in Sc3.4 (Pass 25 at −35%; Pass 303 at −32.4%), before increasing in Sc3.5 (Pass 25 at −13.2%; Pass 303 at −7.6%).

Both passes exhibit strong reductions in water extent when compared to true extent (Fig. 12, red border). In this figure, some regions of the lake, most notably the western part, are filled with unclassified pixels. These areas are unclassified due to the simulator stopping the classification once land pixels surrounding the lake have been labeled. In the case where some areas of emergent riparian vegetation are classified as land, the simulated subscenario shows a reduced water extent. The Sc3.4 results clearly show that if the difference in backscattering values between emergent riparian vegetation and land is small enough, SWOT will falsely classify the emergent riparian vegetation as land. Yet, it remains unclear what degree of difference is required for such a misclassification to occur; further investigation is needed, particularly in wetland regions. Sc3.5 has the second-smallest difference (after Sc3.4) in backscattering values between the emergent riparian vegetation and land (5.21 and 3.03 dB, respectively, which is a very conservative scenario) in comparison to open water or aquatic vegetation. Yet, it still shows a water extent that is closer to true lake extent than the extent without the emergent vegetation, as seen in Sc3.4. These results indicate that SWOT signal attenuation from emergent riparian vegetation can affect the SWOT classification process

if the backscattering difference between emergent riparian vegetation and land is sufficiently small. Such a scenario is foreseeable in wet environments, where soil moisture of land is high, thereby increasing its backscattering intensity and reducing the difference in backscattering values between land and emergent riparian vegetation

Following this logic, it could be expected that Sc3.5 would show the second-smallest extent after Sc3.4, given that it has the second-smallest difference between emergent riparian vegetation and land (5.21 and 3.03 dB, respectively). This is the case for Pass 303, but not for Pass 25. For the latter, Sc3.2 and Sc3.3 exhibit smaller extents than does Sc3.5. A visual inspection reveals that for both Sc3.2 and Sc3.3, a large area of water was classified as land in the western part of Lake Mamawi (Fig. 12). This area of the lake has a complex shoreline and is narrower than the eastern part of the lake. This difference is not only due to emergent riparian vegetation (i.e., low difference water and land backscattering values), but also attributable to incidence angle, since Pass 303 was not affected in the same way. It should be further noted that other studies using the SWOT simulator-HR have witnessed similar problems in complex terrain [9]–[11]. Such differences between passes could become problematic when computing time-series of water volume changes using different passes.

The presence of emergent riparian vegetation could be an area of concern for SWOT, particularly in very wet environments. Since lake size and shape are primary determinants of SWOT storage change accuracy (Lee *et al.* [8]; Solander *et al.* [9]; Bonnema and Hossain [10]; Grippa *et al.* [11]), a decrease in observed surface water extent due to signal attenuation from emergent riparian vegetation could increase the errors on smaller lake observations. Furthermore, the differences in water extent between both passes could be a concern for temporal water storage dynamics calculations. Since the emergent riparian vegetation was most strongly affected when the land cover classification was attributed a relatively high backscattering value, which is indicative of wetter environments (as shown by Sc3.4), it could be expected that the SWOT signal would not be as strongly affected in drier environments, although problems associated with complex shorelines should be investigated further.

C. Further Thoughts

As shown in previous section, the emergent riparian vegetation could have a significant impact on water extent estimated from SWOT. This is an important finding, as it will impact SWOT water storage variation estimates. However, Mamawi Lake is in a particularly wet environment, and it is unclear what percentages of lake in the world seen by SWOT will be affected by emergent riparian vegetation similarly to Mamawi lake. Hence, there is a need to identify lakes in the SWOT a priori lake database [31], where SWOT might show the same issue. Here, the hypothesis is that lakes that have similar emergent riparian vegetation conditions as Mamawi lake are located in wetlands. An attempt was made to compare wetland classifications from the World Wildlife Foundation's Global Lake and Wetland Database (GLWD [32]) with the a priori SWOT lake data base to estimate this percentage globally. Unfortunately, the results are questionable (not presented in this study) because the spatial resolution of the GLWD classes associated to wetland is too coarse. Approaches to delineate emergent riparian vegetation [33], [34] could be used to produce a global high resolution emergent riparian vegetation map and generate quality flags for the SWOT data.

VI. Conclusion

This study has focused upon the affects of aquatic and emergent riparian vegetation on SWOT level 2 products. A land cover classification of Mamawi Lake, which is located in the PAD region (Alberta, Canada), was established using AirSWOT data from summer 2017, with the western portion of the lake being completed with a Landsat 8 image. Using NASA/JPL's SWOT-HR simulator, 10 simulations were performed with varying land cover compositions and backscattering values. Results show that there is little to no effect of aquatic vegetation on SWOT's WSE and water classification. Emergent riparian vegetation may influence SWOT pixel classification when the intensity of the return signal from the land is high (high soil moisture content), with values similar in return signal intensity to emergent riparian vegetation. For most simulations, lake extent reduction varies between 0% and 9%. Simulations with smallest backscattering values between land and emergent riparian vegetation (1.3 dB), however, show a significant reduction in the lake extent (-35%). This level of error could have major effects on the water storage dynamics of lakes in wet environments. Other radar satellite images (with lower electromagnetic frequencies and higher incidence angle), such as the RADARSAT Constellation Mission (RCM) and Sentinel-1 or future missions (e.g., NISAR), could be used to guide the classification process, since they can detect emergent riparian vegetation. Many techniques exist to classify flooded or emergent vegetation using SAR data (e.g., [22]). This could result in higher level products specific to wetland areas. It should be noted that acquisition time differences between SWOT and other SAR missions could vary between none to a several days (e.g., 6 d for Sentinel-1 and 1–4 d for RCM) depending on latitude of the area of interest. However, considering the slow growth rate of vegetation, this time sampling difference should be a minor issue. Further investigation into this problem is required to improve postprocessing strategies for SWOT data in wet environments.

Acknowledgment

The authors would like to thank the Environment and Climate Change Canada, Parks Canada, and the research teams of Laurence Smith (UCLA) and Colin Gleason (University of Massachussets Amherst) for their immense help with fieldwork. SWOT simulations were performed by the Centre Nationale d'Étude Spatiale (CNES). This work is based upon virtual observations with KaRIn, which will be carried aboard SWOT. The JPL is acknowledged for providing binaries of the SWOT simulator that was used in this study and for their help, particularly Brent Williams, in analyzing simulator outputs.

REFERENCES

[1] A. I. Shiklomanov, R. B. Lammers, and C. J. Vörösmarty, "Widespread decline in hydrological monitoring threatens pan-Arctic research," *Eos, Trans. Amer. Geophysical Union*, vol. 83, no. 2, pp. 13–17, 2002, [Online]. Available: https://doi.org/10.1029/2002EO000007

[2] A. K. Mishra and P. Coulibaly, "Developments in hydrometric network design: A review," *Rev. Geophys.*, vol. 47, 2009, Art. no. 2, [Online]. Available: https://doi.org/10.1029/2007RG000243

[3] I. Chawla, L. Karthikeyan, and A. K. Mishra, "A review of remote sensing applications for water security: Quantity, quality, and extremes," *J. Hydrol.*, vol. 585, Jun. 2020, Art. no. 124826, doi: 10.1016/j.jhydrol.2020.124826.

[4] L.-L. Fu, D. Alsdorf, R. Morrow, E. Rodriguez, and N. Mognard, "SWOT: The surface water and ocean topography mission: Wide-swath altimetric elevation on earth," Jet Propulsion Lab., Nat. Aeronautics Space Admin., Pasadena, CA, USA, Technical Report, Feb. 2012. Accessed: Jan. 23, 2021. [Online]. Available: https://trs.jpl.nasa.gov/handle/2014/41996

[5] S. Biancamaria, D. P. Lettenmaier, and T. M. Pavelsky, "The SWOT mission and its capabilities for land hydrology," in *Remote Sensing and Water Resources*. Berlin, Germany: Springer, 2016, pp. 117–147.

[6] E. Rodriguez, "Surface water and ocean topography mission (SWOT): Science requirements document," SWOT NASA/JPL Project, Pasadena, CA, USA, 2015, Accessed: Nov. 1, 2019. [Online]. Available: https://swot.jpl.nasa.gov/files/swot/SRD_021215.pdf

[7] D. Desroches, C. Pottier, D. Blumstein, S. Biancamaria, V. Poughon, and R. Fjortoft, "Large scale pixel cloud simulator and hydrology toolbox," in *Proc. SWOT Sci. Team Meeting*, Montreal, QC, Canada, 2018, Art. no. 23.

[8] H. Lee, M. Durand, H. C. Jung, D. Alsdorf, C. K. Shum, and Y. Sheng, "Characterization of surface water storage changes in Arctic lakes using simulated SWOT measurements," *Int. J. Remote Sens.*, vol. 31, no. 14, pp. 3931–3953, Aug. 2010, doi: 10.1080/01431161.2010.483494.

[9] K. C. Solander, J. T. Reager, and J. S. Famiglietti, "How well will the surface water and ocean topography (SWOT) mission observe global reservoirs?," *Water Resour. Res.*, vol. 52, no. 3, pp. 2123–2140, 2016, [Online]. Available: https://doi.org/10.1002/2015WR017952

[10] M. Bonnema and F. Hossain, "Assessing the potential of the surface water and ocean topography mission for reservoir monitoring in the Mekong river basin," *Water Resour. Res.*, vol. 55, no. 1, pp. 444–461, 2019, [Online]. Available: https://doi.org/10.1029/2018WR023743

[11] M. Grippa *et al.*, "Potential of SWOT for monitoring water volumes in Sahelian ponds and lakes," *IEEE J. Sel. Topics Appl. Earth Observ. Remote Sens.*, vol. 12, no. 7, pp. 2541–2549, Jul. 2019, doi: 10.1109/JSTARS.2019.2901434.

[12] D. E. Fernandez, B. Pollard, P. Vaze, and R. Abelson, "SWOT project mission performance and error budget," in *Proc. IEEE Int. Geosci. Remote Sens. Symp.*, 2017, pp. 8625–8628.

[13] M. C. Kestwal, S. Joshi, and L. S. Garia, "Prediction of rain attenuation and impact of rain in wave propagation at microwave frequency for tropical region (Uttarakhand, India)," *Int. J. Microw. Sci. Technol.*, vol. 2014, pp. 1–6, Jun. 2014, doi: 10.1155/2014/958498.

[14] L. C. Smith *et al.*, "AirSWOT flights and field campaigns for the 2017 Arctic-Boreal vulnerability experiment (ABoVE)," *AGU Fall Meeting Abstr.*, vol. 21, Dec. 2017, Accessed: Jan. 23, 2021. [Online]. Available: http://adsabs.harvard.edu/abs/2017AGUFM.C21F1176S

[15] E. H. Altenau *et al.*, "AirSWOT measurements of river water surface elevation and slope: Tanana River, AK," *Geophysical Res. Lett.*, vol. 44, no. 1, pp. 181–189, 2017.

[16] M. Denbina, M. Simard, E. Rodriguez, X. Wu, A. Chen, and T. Pavelsky, "Mapping water surface elevation and slope in the Mississippi River delta using the AirSWOT Ka-band interferometric synthetic aperture radar," *Remote Sens.*, vol. 11, Jan. 2019, Art. no. 23, doi: 10.3390/rs11232739.

[17] J. V. Fayne *et al.*, "Airborne observations of Arctic-Boreal water surface elevations from AirSWOT Ka-band InSAR and LVIS LiDAR," *Environ. Res. Lett.*, vol. 15, no. 10, Oct. 2020, Art. no. 105005, doi: 10.1088/1748-9326/abadcc.

[18] S. Tuozzolo *et al.*, "Estimating river discharge with swath altimetry: A proof of concept using AirSWOT observations," *Geophysical Res. Lett.*, vol. 46, no. 3, pp. 1459–1466, 2019, [Online]. Available: https://doi.org/10.1029/2018GL080771

[19] E. D. Kyzivat *et al.*, "A high-resolution airborne color-infrared camera water mask for the NASA ABoVE campaign," *Remote Sens.*, vol. 11, no. 18, Jan. 2019, Art. no. 18, doi: 10.3390/rs11182163.

[20] L. H. Pitcher *et al.*, "AirSWOT InSAR mapping of surface water elevations and hydraulic gradients across the Yukon Flats basin, Alaska," *Water Resour. Res.*, vol. 55, no. 2, pp. 937–953, 2019, [Online]. Available: https://doi.org/10.1029/2018WR023274

[21] R. Fjortoft *et al.*, "KaRIn on SWOT: Characteristics of near-Nadir Ka-band interferometric SAR imagery," *IEEE Trans. Geosci. Remote Sens.*, vol. 52, no. 4, pp. 2172–2185, Apr. 2014.

[22] V. Tsyganskaya, S. Martinis, P. Marzahn, and R. Ludwig, "SAR-based detection of flooded vegetation–A review of characteristics and approaches," *Int. J. Remote Sens.*, vol. 39, no. 8, pp. 2255–2293, 2018.

[23] F. Mohammadimanesh, B. Salehi, M. Mahdianpari, B. Brisco, and M. Motagh, "Wetland water level monitoring using interferometric synthetic aperture radar (InSAR): A review," *Can. J. Remote Sens.*, vol. 44, no. 4, pp. 247–262, 2018.

[24] J. V. Fayne *et al.*, "Airborne observations of Ka-band radar backscatter from AirSWOT enable vegetation and water detection," in *Proc. AGU Fall Meeting 2020*, Dec. 2020. Accessed: Feb. 17, 2021. [Online]. Available: https://agu.confex.com/agu/fm20/meetingapp.cgi/Paper/684541

[25] D. L. Peters, T. D. Prowse, A. Pietroniro, and R. Leconte, "Flood hydrology of the Peace-Athabasca Delta, Northern Canada," *Hydrological Processes*, vol. 20, no. 19, pp. 4073–4096, 2006, [Online]. Available: https://doi.org/10.1002/hyp.6420

[26] A. Pietroniro *et al.*, "Canada's contributions to the SWOT mission – terrestrial Hydrology (SWOT-C TH)," *Can. J. Remote Sens.*, vol. 45, no. 2, pp. 116–138, Mar. 2019, doi: 10.1080/07038992.2019.1581056.

[27] J. Bergeron, G. Siles, R. Leconte, M. Trudel, D. Desroches, and D. L. Peters, "Assessing the capabilities of the SWOT mission for large lake water surface elevation monitoring under different wind conditions," *Hydrol. Earth Syst. Sci. Discuss.*, vol. 24, pp. 5985–6000, Jun. 2020. [Online]. Available: https://doi.org/10.5194/hess-2020-162

[28] A. Domeneghetti *et al.*, "Characterizing water surface elevation under different flow conditions for the upcoming SWOT mission," *J. Hydrol.*, vol. 561, pp. 848–861, 2018.

[29] M. Durand *et al.*, "How will radar layover impact SWOT measurements of water surface elevation and slope, and estimates of river discharge?," *Remote Sens. Environ.*, vol. 247, Sep. 2020, Art. no. 111883, doi: 10.1016/j.rse.2020.111883.

[30] E. Peral and D. Esteban-Fernandez, "SWOT mission performance and error budget," in *Proc. IEEE Int. Geosci. Remote Sens. Symp.*, Jul. 2018, pp. 8625–8628, doi: 10.1109/IGARSS.2018.8517385.

[31] Y. Sheng *et al.*, "Representative lake water extent mapping at continental scales using multi-temporal Landsat-8 imagery," *Remote Sens. Environ.*, vol. 185, pp. 129–141, Nov. 2016, doi: 10.1016/j.rse.2015.12.041.

[32] B. Lehner and P. Döll, "Development and validation of a global database of lakes, reservoirs and wetlands," *J. Hydrol.*, vol. 296, no. 1, pp. 1–22, Aug. 2004, doi: 10.1016/j.jhydrol.2004.03.028.

[33] V. Klemas, "Remote sensing of emergent and submerged wetlands: An overview," *Int. J. Remote Sens.*, vol. 34, no. 18, pp. 6286–6320, Sep. 2013, doi: 10.1080/01431161.2013.800656.

[34] L. Huylenbroeck, M. Laslier, S. Dufour, B. Georges, P. Lejeune, and A. Michez, "Using remote sensing to characterize riparian vegetation: A review of available tools and perspectives for managers," *J. Environ. Manage.*, vol. 267, Aug. 2020, Art. no. 110652, doi: 10.1016/j.jenvman.2020.110652.

Nicolas M. Desrochers received the B.A. degree in geography in 2015 from Ottawa University, Ottawa, ON, Canada, where he worked on paleoflood reconstruction from Oxbow lakes, and the M.Sc. degree in geographical sciences in 2017 from Université de Sherbrooke, Sherbrooke, QC, Canada, where he worked on the calibration of hydraulic models using high-resolution synthetic aperture radar data. He is currently working toward the Ph.D. degree in civil engineering with Université de Sherbrooke, where he focuses on the application of remotely sensed data for water resource management.

He worked on paleoflood reconstruction from oxbow lakes with Ottawa University. He also worked on the calibration of hydraulic models using high resolution synthetic aperture radar data with the Université de Sherbrooke.

Mélanie Trudel received the B.Sc. degree in physics from Université de Montréal, Montreal, QC, Canada, in 2004, the M.Sc. degree in geosciences from Université de Sherbrooke, Sherbrooke, QC, Canada, in 2006, and the Ph.D. degree in civil engineering from École de technologie supérieure, Montreal, QC, Canada, in 2010.

In 2010, she was a Postdoctoral Researcher with Université de Sherbrooke, where in 2017, she was a Professor with the Civil and Building Engineering Department. Since 2014, she has been involved in SWOT studies through collaboration with the Canadian Space Agency. Her research interests focus, among others, on the use of remote sensing for water resources (soil moisture, snow, and water levels).

Sylvain Biancamaria received the M.Eng. degree in remote sensing data processing from Supaero, Toulouse, France, in 2005, and the M.Sc. degree in geosciences and the Ph.D. degree in hydrology from the University of Toulouse, Toulouse, France, in 2006 and 2009, respectively.

In 2010, he was a Postdoctoral Researcher with the University of Washington, Seattle, WA , USA. In 2011, he joined the French National Center for Scientific Research, as a Research Scientist with LEGOS, Toulouse, France. He has been on the SWOT Science Team since 2013. His research interests include water surface study using models, *in situ* and remote sensing data to analyze causes and consequences of water storage and fluxes variabilities of watersheds.

Gabriela Siles received the Ingeniero degree in geodesy and geophysics from the National University of Tucuman, Tucumán, Argentina, in 2011 and the Ph.D. in engineering from the Technical University of Braunschweig, Braunschweig, Germany, in 2015.

She was a Postdoctoral Fellow with the University of Sherbrooke, Sherbrooke, QC, Canada, and was a casual Physical Scientist for Environment and Climate Change Canada. She is currently a Research Associate with the University of Sherbrooke. Her research interests include optical and radar imagery, and satellite altimetry for water resources and in water modeling.

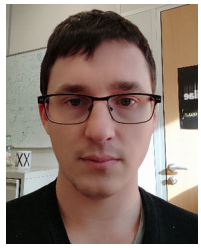

Damien Desroches was born in Limoges, France, in 1989. He received the Ph.D. degree in climate, ocean, atmosphere, and continentals surfaces from l'Université Toulouse III Paul Sabatier, Toulouse, France, in 2016.

In 2016, he joined the French Space Agency Centre National d'études Spatiales, Toulouse, France, where he is currently a Radar Engineer with the Radar Processing Department. He is currently developing radar simulators and processing algorithms for the SWOT mission, in cooperation with NASA's Jet Propulsion Laboratory.

Denis Carbonne received the B.Sc. degree in electrical engineering from Ecole Nationale de l'Aviation Civile, Toulouse, France, in 1988.

Since 1989, he has been with Centre National d'études Spatiales Toulouse Space Center, Toulouse, France, where he has been in charge of antennas development, and then spaceflight dynamics mission design and in-orbit-transfer operations. Since 2014, he has been with Radar and Altimetry Processing Department, involved in SWOT Karin instrument processing chain development, and other radar interferometry applications.

Robert Leconte received the Ph.D. degree in civil and environmental engineering from Utah State University, Logan, UT, USA, in 1987.

He is currently a full-time Professor with the Université de Sherbrooke, Sherbrooke, QC, Canada. He currently holds an Industrial Research Chair funded by the National Science and Engineering Research Council of Canada on the applications of remote sensing for water resources. His research interests include encompass hydrology, hydrological modeling, climate change impacts on water resources and remote sensing applications in hydrological modeling and forecasts, for which he has been involved for more than 25 years.